LANGMUIR

pubs.acs.org/Langmuir Article

Growth of Crystalline Bimetallic Metal–Organic Framework Films via Transmetalation

Amy J. Brandt, Deependra M. Shakya, Kamolrat Metavarayuth, Ekaterina Dolgopolova, Lauren Hensley, Audrey S. Duke, Sharfa Farzandh, Morgan Stefik, Natalia B. Shustova,* and Donna A. Chen*

Cite This: *Langmuir* 2020, 36, 9900–9908 Read Online

ACCESS | Metrics & More | Article Recommendations | Supporting Information

ABSTRACT: Crystalline films of the $Cu_3(BTC)_2$ (BTC^{3-} = 1,3,5-benzenetricarboxylate) metal–organic framework (MOF) have been grown by dip-coating an alumina/Si(111) substrate in solutions of Cu(II) acetate and the organic linker H_3BTC. Atomic force microscopy (AFM) experiments demonstrate that the substrate is completely covered by the MOF film, while grazing incidence wide-angle X-ray scattering (GIWAXS) establishes the crystallinity of the films. Forty cycles of dip-coating results in a film that is ∼70 nm thick with a root mean squared roughness of 25 nm and crystallites ranging from 50–160 nm in height. Co^{2+} ions were exchanged into the MOF framework by immersing the $Cu_3(BTC)_2$ films in solutions of $CoCl_2$. By varying the temperature and exchange times, different concentrations of Co were incorporated into the films, as determined by X-ray photoelectron spectroscopy experiments. AFM studies showed that morphologies of the bimetallic films were largely unchanged after transmetalation, and GIWAXS indicated that the bimetallic films retained their crystallinity.

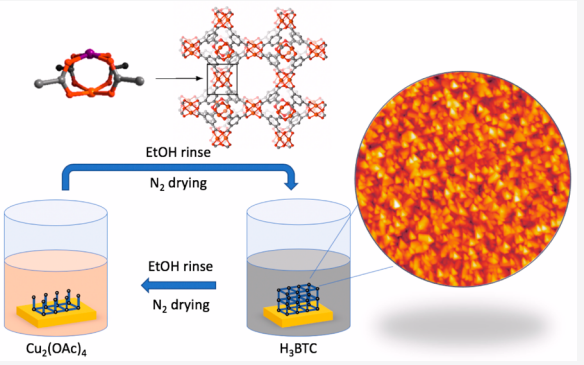

INTRODUCTION

Based on their tunable, porous structures and diversity of metal nodes, metal–organic frameworks (MOFs) have attracted interest for many applications, including catalysis,[1−6] gas storage and separations,[7−11] energy transfer,[12,13] and sensing devices.[14−16] Furthermore, tuning the electronic properties of MOFs by modifying their modular framework has become a promising area of research.[14,15] The incorporation of a second metal into the framework through metal node modification or ligand extension has been studied as a means to promote desirable chemical and electronic properties.[17−21] For example, our group has demonstrated that $(Cu_xCo_{1-x})_3(BTC)_2$ (abbreviated as CuCoBTC) exhibits unusual electronic properties compared to pure $Cu_3(BTC)_2$ (HKUST-1, abbreviated as CuBTC), as demonstrated by the shift of the valence band edge toward the Fermi level.[17] In addition, when Rh ions are exchanged into the CuBTC framework, the resulting CuRhBTC MOF shows activity for propylene hydrogenation with the Rh^{2+} ions serving as active sites.[22]

Traditional synthesis techniques using solvothermal methods result in the fabrication of MOFs in the form of powders. However, the growth of crystalline MOF films provides the opportunity for fundamental studies involving systematic control of chemical and electronic properties as a function of the incorporation of a second metal into the MOF framework. Specifically, catalytic reactions such as hydrogenation, oxidation, and epoxidation are known to occur at the MOF metal nodes;[1,9,22−25] the kinetics of these reactions can be more effectively studied on well-defined, MOF thin films rather than on MOF powders, where diffusion of species within the pores may play a role. Films also provide the structural uniformity necessary for use in MOF-based devices such as in photovoltaics, sensors, and thermoelectrics.[16,26−30] Most recently, the development of MOFs as thin films has garnered significant attention for electrochemical applications.[31−39]

The method by which the MOF film is grown is key to the integrity of its structure and the resulting performance.[26,30,40−42] Growth procedures such as solvothermal film synthesis, in which the substrate is heated in a solution of precursors,[30,42−44] deposition of a presynthesized MOF powder onto the substrate material by drop-casting,[30,39,42,45] or electrodeposition[30,37,38,42] often lead to polycrystalline films with poor adhesion between the MOF and the underlying substrate. A number of studies have reported the use of self-assembled monolayers (SAMs) for functionalizing the substrate surface and serving as a foundation for MOF film growth.[42,46−49] Among the many strategies for MOF film

Received: May 25, 2020
Revised: July 13, 2020
Published: July 15, 2020

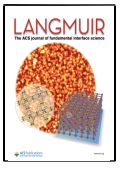

https://dx.doi.org/10.1021/acs.langmuir.0c01535
Langmuir 2020, 36, 9900–9908

synthesis, Wöll and co-workers developed a layer-by-layer deposition procedure using SAMs to anchor the film to the substrate,[42,47,50−54] and this approach is notable for producing highly ordered, crystalline films that allow for control over the film thickness. Limited thermal and chemical stability are disadvantages of using SAMs for binding the MOF precursors to the support,[42,55] but Stavila et al. reported that crystalline CuBTC films could be grown directly on alumina and silica surfaces using this layer-by-layer deposition approach.[15]

Although the incorporation of a second metal in the MOF structure is known to improve catalytic, conductive, and gas storage properties for MOF powders,[17,19,56−59] the field of bimetallic MOF thin films has been relatively unexplored, particularly for two different metals incorporated at the same type of metal node. A number of bimetallic MOF films have been constructed from one type of metal at the node and a different metal incorporated into the associated ligands.[31,32,34,36,38,44,60] In other studies, metallic complexes have been selectively deposited at MOF nodes,[61,62] and these techniques have been extended to selective deposition of complexes at the Zr_6 nodes of NU-1000 thin films.[59,60,63] Bimetallic MOF films have also been prepared from solvothermal synthesis,[38,64] in which the preformed MOF powders are coated onto the substrate in a thin layer,[39,45] and from electrochemical deposition.[37] Kitagawa et al. grew bimetallic MOF thin films consisting of cyanide-bridged 2D layers containing Fe^{2+} and $M(CN)_4$ (M = Ni,[65] Pd,[66] Pt[67−69]) connected by pyrazine, pyridine, or bipyridine ligands to form a 3D lattice; notably, the growth of these bimetallic films involved thiol-based self-assembled monolayers (SAMs) for film nucleation and orientation, and therefore, the thermal stability of the films is limited by decomposition temperature of the SAMs.

In this work, we present the first study of crystalline, bimetallic MOF films prepared by growth of a monometallic MOF film (CuBTC) followed by transmetalation for incorporation of a second metal (Co^{2+}) at the paddle-wheel nodes. For MOF powders, different metal ions have been successfully exchanged into the CuBTC framework by exposure to a solution of the second metal ion (Co,[17] Rh,[22] Ru,[70] Ni,[22] Ir,[22] and Zn[17]). The CuBTC MOF was chosen for initial film growth based on its desirable qualities of high surface area, good thermal stability, and stability in air.[71] Furthermore, there are a number of different methods reported in the literature that have been successful in growing crystalline CuBTC films.[30,41,72−74] Cobalt was selected as the second metal based on the unusual electronic properties observed for the CuCoBTC MOF in its powder form.[17] From a catalytic perspective, Co-containing MOFs also exhibit desirable activity in electrochemical reactions.[33,35,45,60,75]

In the first step of our MOF thin film synthesis, crystalline films of CuBTC are grown on an alumina/Si(100) substrate by dip-coating in alternating solutions of copper acetate and organic linker (1,3,5-benzenetricarboxylic acid). A thin (2.5 nm) alumina film was chosen as the substrate, given that oxide surfaces like alumina and silica provide native surface hydroxyl groups that initiate MOF film growth.[15] In the second step, Co^{2+} ions are exchanged into the MOF framework by immersing the CuBTC films in solutions of $CoCl_2$. By varying the temperature and immersion time for exchange, different concentrations of Co are incorporated into the films, as determined by X-ray photoelectron spectroscopy (XPS) experiments. Atomic force microscopy (AFM) measurements show that the substrate is uniformly covered by the MOF film after transmetalation, and grazing incidence wide-angle X-ray scattering (GIWAXS) studies confirm that the bimetallic films retain their crystallinity. Stability studies of the films stored under *N,N′*-dimethylformamide (DMF) demonstrate that the coverage remains uniform with crystallites completely covering the surface although some rearrangement occurs as the crystallite sizes increase over time.

EXPERIMENTAL SECTION

Materials. $Cu(CH_3COO)_2{\cdot}H_2O$ ($Cu(OAc)_2$, >95%, TCI America), 1,3,5-benzenetricarboxylic acid (H_3BTC, 98%, Alfa Aesar), $CoCl_2{\cdot}6H_2O$ (>98.0%, TCI America), ethanol (200 proof, Decon Laboratories), *N,N′*-dimethylformamide (DMF, ACS grade, BDH), trichloroethylene (99.9%, BDH), acetone (≥99.5%, Sigma-Aldrich), and methanol (≥99.8%, Sigma-Aldrich) were used as received.

Film Synthesis. Thin films of CuBTC were grown on a sputter-deposited 2.5 nm film of Al_2O_3 on a polished, p-type Si(100) substrate (University Wafer). The wafer substrates were cut into 1.0 cm × 1.2 cm rectangles and thoroughly cleaned by sonication in trichloroethylene, acetone, and methanol for 20 min in each solvent. The precursors for growing the CuBTC films consisted of 1 mM $Cu(OAc)_2$ in ethanol and 1 mM H_3BTC in ethanol. The substrate was first immersed in the $Cu(OAc)_2$ solution for 1 min followed by a 15 s rinse in ethanol and 15 s of drying under a flow of N_2. The substrate was then immersed in H_3BTC solution for 1 min followed by a 15 s rinse in ethanol and 15 s of drying under N_2. This process of exposure to $Cu(OAc)_2$/ethanol−N_2/H_3BTC/ethanol−N_2 constituted one growth cycle. Forty cycles were used for the synthesis of each CuBTC film unless otherwise specified.

Film Transmetalation. Bimetallic CuCoBTC films were prepared by exposing the CuBTC film to a $CoCl_2$ solution in DMF (10 mL, 1.05 g of $CoCl_2$) or ethanol (10 mL, 0.33 g of $CoCl_2$). The length of time (0.25−24 h) and temperature of transmetalation (25−90 °C) determined how much Co^{2+} was exchanged into the CuBTC film. After the metal exchange, the bimetallic film was placed either in DMF or ethanol to remove excess $CoCl_2$. DMF was chosen as an exchange solvent based on the known procedure for transmetallating Co^{2+} into the CuBTC framework for MOF powders.[17] Ethanol was also investigated as an exchange solvent since the CuBTC films were grown from ethanolic solutions, but the boiling point of ethanol limited transmetalation temperatures to 70 °C or lower. In these studies, DMF can be assumed to be the exchange solvent unless otherwise stated. The details of the preparation of all films shown in the figures are given in Table S1.

Characterization. X-ray photoelectron spectroscopy (XPS) data were collected using a Kratos AXIS Ultra DLD system with a monochromatic Al Kα source, hemispherical analyzer, and charge neutralizer.[17,76] The base pressure of the vacuum chamber was 1 × 10^{-9} Torr before sample introduction and ≤3 × 10^{-9} Torr during experiments. The dwell time for all regions was 1000 ms, and the energy step size was 0.06 eV. Survey scans were collected for all films to ensure that there were no contaminants introduced during sample preparation. Absolute binding energies were determined by setting the position of the lower energy adventitious carbon peak to 284.8 eV. Metal compositions for the bimetallic films were determined from the integrated areas of the Co($2p_{3/2}$) and Cu($2p_{3/2}$) peaks and the relative sensitivity factors for Cu and Co. The relative sensitivity factors from the Kratos Vision software were used for the Co($2p_{3/2}$), Cu($2p_{3/2}$), and Cl(2p) regions (2.393, 3.547, and 0.48, respectively). The baseline chlorine signal for all films, including CuBTC, ranged from zero to no more than 6% of the Cu(2p) signal.

Grazing incidence wide-angle X-ray scattering (GIWAXS) data were collected on a SAXSLab Ganesha instrument at the South Carolina SAXS Collaborative. A Xenocs GeniX3D microfocus source with a Cu target and a Hybrid Pixel Array Pilatus detector (Dectris) were used for collecting scattering patterns. Measurements of films were conducted for 30 min at an incident angle of 4° while at room temperature.

https://dx.doi.org/10.1021/acs.langmuir.0c01535
Langmuir 2020, 36, 9900−9908

Tapping mode atomic force microscopy (AFM) experiments were carried out in air using a Multimode Nanoscope IIIA system (Digital Instruments Inc.) with commercial Si cantilevers (ACT, Applied NanoStructures) at a scan rate of 1 Hz. Analysis of crystallite heights, root mean squared surface roughness, and fraction of the surface covered by crystallites was carried out using the shareware program Image SXM. For the latter measurements on the 10 and 20 cycle films, bare substrate regions could clearly be identified based on the flatness of these regions and their consistent relative heights. In the case of the 40 cycle films, it was less clear that the low points on the surface were exposed substrate, and therefore, the fraction of the surface covered by crystallites may be underestimated.

MOF film thicknesses were measured with a field emission scanning electron microscope (Zeiss Gemini Ultraplus). The edge of the MOF film was coated with gold (200 Å) to prevent charging effects.

RESULTS AND DISCUSSION

GIWAXS: Crystallinity. GIWAXS data for the CuBTC films grown by dip-coating are consistent with the known crystal structure of CuBTC powders reported in the literature (Figure 1).[71] A simulated pattern for CuBTC is shown in the top panel of Figure 1 along with the assignments for the prominent peaks at the lower scattering angles. The CuCoBTC films prepared by exchanging Cu^{2+} with Co^{2+} ions at different temperatures and times (19−66%, Figure 1) also show GIWAXS patterns that are anaologous to the CuBTC film, indicating that the crystallinity of the film is retained after incorporation of Co into the MOF structure. The diffraction patterns after Co^{2+} addition are shifted slightly toward higher diffraction angles; however, this change was within the ∼2 degrees of error associated with the grazing incidence sample alignment and calibration drift. The film in which 100% of the Cu^{2+} ions were exchanged for Co^{2+} did not exhibit the CuBTC structure (Figure 1), indicating that some fraction of Cu^{2+} is necessary to stabilize the framework. In general, the CuCoBTC films were found to be crystalline for Co concentrations ranging from 10% to 96%.

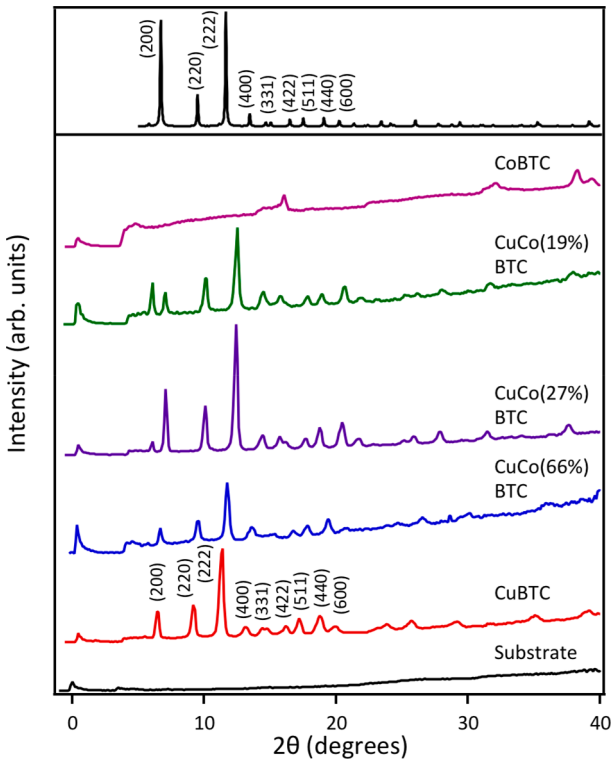

Figure 1. GIWAXS data for the Al_2O_3/Si substrate (black); CuBTC film (red); CuCoBTC film (66% Co, exchanged at 90 °C for 15 min, blue); CuCoBTC film (27% Co, exchanged at 50 °C for 60 min, purple); CuCoBTC film (19% Co, exchanged at 25 °C for 24 h in ethanol, green); and CoBTC film (100% Co, exchanged at 90 °C for 8 h, pink). As a reference, the top panel shows the simulated pattern for CuBTC.

XPS: Surface Composition and Oxidation States. The Co concentrations in the CuCoBTC films as a function of exchange time, temperature, and solvent are shown in Figure 2.

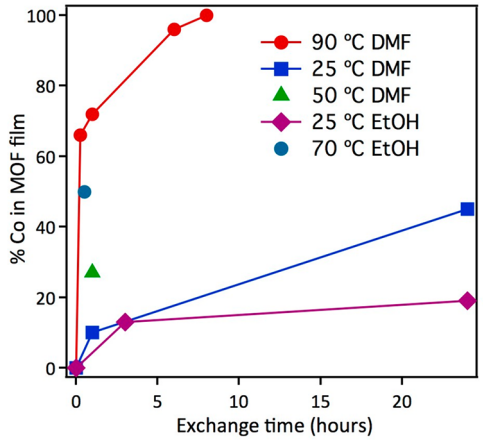

Figure 2. Plot of percent Co incorporation into the framework as a function of exchange time at various temperatures in DMF and ethanol solvents.

The relative Co/Cu compositions were established from the integrated $Co(2p_{3/2})$ and $Cu(2p_{3/2})$ peaks after correcting for atomic sensitivities. Co concentrations across the films were found to be consistent based on the sampling of the 72% CuCoBTC film at three different areas, which had a standard deviation of 4%. The general trend is that greater incorporation of Co into the framework is achieved at longer exchange times and higher temperatures. At the highest temperature studied (90 °C in DMF), Co exchange is 66% after only 15 min, and nearly 100% exchange is achieved after 6 h. At a lower temperature of 50 °C, 27% exchange occurs after 1 h, and this value drops to 10% for the same conditions at 25 °C. Furthermore, only 45% Co is reached after 24 h at 25 °C in DMF, and with ethanol as a solvent, the Co composition is even lower at 19%. This is presumably a result of the lower concentration of $CoCl_2$ in the exchange solution due to the lower solubility in ethanol. Higher concentrations of 50% Co can still be achieved at elevated temperature (70 °C) after 0.5 h in ethanol solution, but the maximum exchange temperature is limited by the lower boiling point of ethanol compared to DMF.

XPS data for CuBTC and CuCoBTC films are presented in Figure 3. The Al_2O_3/Si substrate itself had no features in the Co(2p) and Cu(2p) regions, and the CuBTC film did not exhibit features in the Co(2p) region (Figure 3a, b). Notably, significant intensity in the Cl(2p) region (186−206 eV) was not detected for the exchanged films, and this eliminates the possibility that $CoCl_2$ is retained in the pores of the MOF film or adsorbed on the surface rather than having Co^{2+} exchanged with Cu^{2+} ions in the framework. For the 45%, 66%, and 72%

https://dx.doi.org/10.1021/acs.langmuir.0c01535
Langmuir 2020, 36, 9900−9908

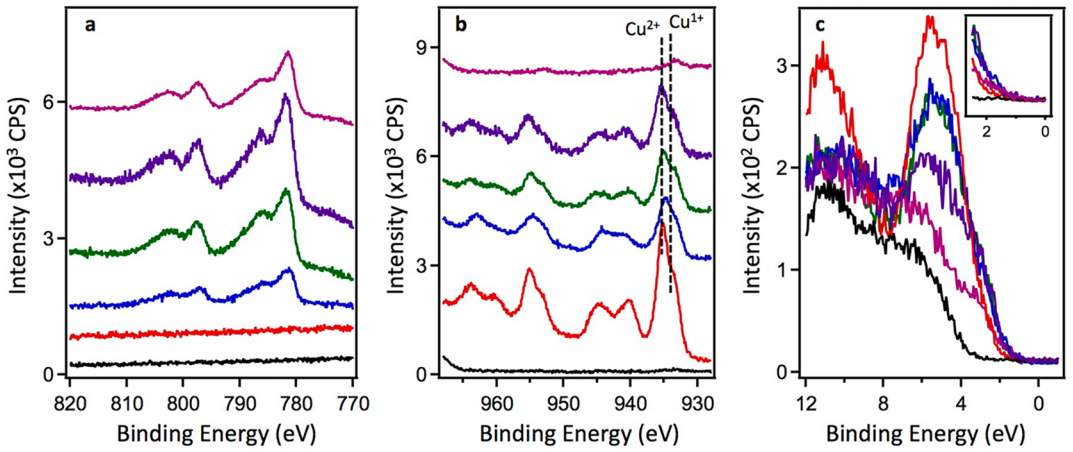

Figure 3. XPS data for (a) Co(2p), (b) Cu(2p), and (c) valence band regions. Surfaces shown are the Al_2O_3/Si substrate (black), CuBTC film (red), CuCoBTC film (45% Co, blue), CuCoBTC film (66% Co, green), CuCoBTC film (72% Co, purple), and CuCoBTC film (96% Co, pink). The inset for (c) is an expanded region at the valence band edge.

CuCoBTC films, the Co($2p_{3/2}$) peak appeared at 781.8 eV, which is the same as the binding energy attributed to Co^{2+} for CuCoBTC MOF powders.[17] The pronounced shoulder at 4−5 eV higher binding energy is ascribed to final state effects and core-hole screening associated with charge transfer from the ligand to the 3d orbitals;[77,78] this satellite feature is associated with paramagnetic Co^{2+},[79,80] which is also consistent with the 16 eV splitting between the Co($2p_{3/2}$) and Co($2p_{1/2}$) peaks, as opposed to a splitting of 15 eV observed for diamagnetic Co^{3+}.[81,82] In the Cu(2p) region (Figure 3b), the CuBTC film has a peak at 935.2 eV assigned to Cu^{2+} and a shoulder at 933.5 eV assigned to Cu^{1+}.[76] A combination of removal of the coordinating solvent/water in vacuum and irradiation by X-rays is known to induce reduction of Cu^{2+} to Cu^{1+} in CuBTC.[76,83] Furthermore, the satellite features at 940.2 and 944.9 eV are also characteristic of Cu^{2+} and not observed for Cu^{1+}.[76] Given that the Cu($2p_{3/2}$) binding energies are nearly identical for Cu^0 and Cu^{1+},[84,85] the Cu(LMM) Auger region was collected (Figure S1) to confirm that metallic Cu was not present. Cu^0 should appear as a sharp peak at ∼567 eV, which is not observed in our samples; instead, the Cu(LMM) spectra for the films show a broader feature at 572 eV associated with Cu^{1+}.[86] For the CuCoBTC films containing 45−66% Co, the main features in the Cu(2p) region are the same as for CuBTC although the intensities decrease due to the lower Cu concentration. For the CuCoBTC film with only 4% Cu, the main peak appears to be Cu^{1+}.

Valence band spectra (Figure 3c) demonstrate that incorporation of Co into the MOF results in a shift in the valence band edge to lower binding energies. While the insulating Al_2O_3/Si substrate has almost no intensity above 4 eV, the CuBTC film has a peak in the valence band region at 5.25 eV as well as intensity that extends to ∼2 eV. The valence band spectra for the CuCoBTC films (45−72% Co) are similar to that of CuBTC except that the valence band edge extends slightly more toward the Fermi level for the bimetallic films. For example, the onset of the rise of the valence band edge occurs at ∼0.7 eV lower in energy for the 72% Co film compared to CuBTC. The 96% Co film has a peak shape that resembles that of the substrate except at binding energies ≤4 eV, where a higher intensity tail exists, and this behavior is attributed to the fact that the 96% Co film has some regions of exposed substrate. Previous studies of CuCoBTC MOF powders have shown that the valence band edge shifts significantly toward the Fermi level compared to the position for the CuBTC valence band edge, indicating that there is a greater density of states near the Fermi level, as typically observed for a semiconductor.[17] However, for the CuCoBTC films, differences in the valence band edge compared to CuBTC are not as pronounced, and intensity does not appear at the Fermi level.

The C(1s) and O(1s) XPS data for the MOF films are consistent with what has been previously reported for the MOF powders (Figure S1).[17,76] The higher binding energy C(1s) peak at 288.8 eV is attributed to C═O while the 284.8 eV is assigned to a combination of adventitious carbon and aliphatic carbons. For both MOF films and powders, the ratio of the 288.8 to 284.8 eV peaks is 0.32 ± 0.04. In the cases where the MOF films are partially delaminated, this ratio decreases and is therefore used as an indicator of delamination, which we define as separation of the film from the substrate. The 96% Co film is believed to be partially delaminated given that this ratio is 0.26. Furthermore, the Al(2s) and Si(2p) signals from the substrate are visible, whereas these signals are almost completely attenuated for the CuBTC films. The shape of the O(1s) peak is also indicative of exposed Al_2O_3 regions since oxygen species in the MOFs have a narrower O(1s) peak, and oxygen in alumina is shifted to lower binding energy by 0.4 eV. In general, delamination of the films is characterized by more prominent Si(2p) and Al(2s) peaks from the substrate, as well as a decrease in MOF/adventitious carbon ratio and a broadening and shift to lower binding energy for the O(1s) peak. Notably, the GIWAXS data for the partially delaminated films indicate that they are still crystalline. The extent of film delamination tends to increase with increasing Co concentration and is attributed to the following reasons. First, the more aggressive exchange conditions (longer times at high temperature) required for the higher Co concentrations weaken the adhesion between the film and substrate. Second, the crystalline CuCoBTC films are expected to be less stable than CuBTC and, therefore, more prone to degradation and dissolution; cluster structures consisting of dimetal paddle-wheel nodes connected by carboxylate linkers are reported to be more stable for Cu^{2+} in the paddle-wheel compared with Co^{2+}.[87−89]

https://dx.doi.org/10.1021/acs.langmuir.0c01535
Langmuir 2020, 36, 9900−9908

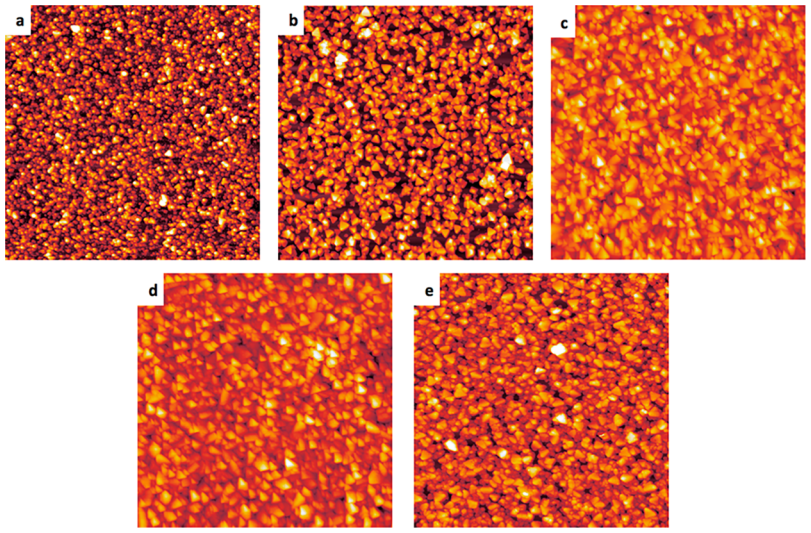

Figure 4. AFM images of CuBTC films grown by (a) 10 dip-coating cycles, (b) 20 dip-coating cycles, and (c) 40 dip-coating cycles and of CuCoBTC films for (d) 66% Co, exchanged at 90 °C for 15 min, and (e) 72% Co, exchanged at 90 °C for 60 min. Both CuCoBTC films were grown from CuBTC films with 40 cycles of dip-coating. All images are 5 μm × 5 μm, and vertical scale bars are provided in Figure S3.

AFM and SEM: Film Morphologies and Thicknesses. AFM experiments were conducted to characterize the morphology of the MOF films. Films prepared by 10 dip-coating cycles resulted in crystallites 20−60 nm high and 60−180 nm wide, whereas a 20 cycle film resulted in features 35−95 nm high and 80−245 nm wide (Figure 4a, b). The surfaces of the CuBTC films grown by 40 dip-coating cycles appear to be almost completely covered by crystallites with lateral dimensions ranging from 200−400 nm and heights of 60−150 nm (Figure 4c); the root mean squared (RMS) roughness was ∼25 nm. For the 10 and 20 cycle films ∼30% of the substrate was exposed compared to <5% for the 40 cycle film based on an analysis of the AFM images (see Experimental Section). Therefore, a smaller number of dip-coating cycles resulted in thinner films, but complete coverage of the surface was not achieved. For the standard CuBTC films grown by 40 dip-coating cycles, film thicknesses were estimated as ∼70 nm from cross-sectional SEM measurements that were taken from a set of 13 images, in which films of uniform thickness could be observed (Figure S2). Typical film thicknesses ranged from 40 to 105 nm with an average value of 70 nm, and these values are in reasonable agreement with the crystallite heights measured by AFM. After a CuBTC film was exchanged in $CoCl_2$ solution for 15 min at 90 °C to produce a 66% Co concentration, the overall morphology of the film was unchanged, and the RMS roughness remained 25 nm (Figure 4d). Furthermore, a longer exchange time of 1 h at 90 °C, which produced a film with 72% Co, had similar crystallite sizes and RMS roughness (∼35 nm, Figure 4e). Thus, incorporation of Co into the MOF film did not alter the overall film morphology.

Films were also exchanged using ethanol as a solvent instead of DMF. The films exchanged in ethanol exhibited smaller crystallites with widths and heights of roughly 75 and 20 nm, respectively, although some larger crystallites ∼200 nm in width and ∼70 nm in height also formed (Figure 5). The RMS roughness of the ethanol-exchanged films was 13−17 nm, which was lower than those exchanged in DMF. These results therefore suggest that exposure of the MOF to DMF facilitates larger crystallite sizes whereas exposure to ethanol results in distinctly smaller crystallites. Although the imaged film morphologies can be strongly influenced by the shape of the AFM tip, the faceted shapes of the crystallites in Figures 4 are believed to be real, given that imaging with different AFM tips yielded the same results. Moreover, the same AFM tips that imaged faceted crystallites exchanged in DMF showed less regular features for the films exchanged in ethanol.

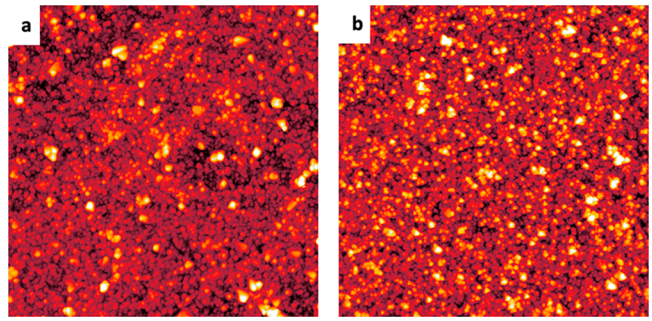

Figure 5. AFM images of CuCoBTC films (a) 13% Co, exchanged at 25 °C for 3 h in ethanol, and (b) 50% Co, exchanged at 70 °C for 30 min in ethanol. All images are 5 μm × 5 μm.

Surface morphologies of the films were preserved by storing them in closed vials that were purged with N_2 gas, but when the films were stored under DMF, delamination occurred over time. Figure 6a shows a CuBTC film that was stored under DMF for 40 days; the dimensions of these crystallites, which ranged from 150−425 nm in width and 32−150 nm height, were much larger than the ones observed for the freshly grown film (Figure 4a) and suggest that DMF promotes restructuring of CuBTC into larger crystallites. Furthermore, AFM images for a CuCoBTC film (10% Co, exchanged 1 h in DMF) that was stored for 22 days in DMF (Figure 6b) exhibited the same large crystallites observed in Figure 6a for CuBTC under DMF. This is not an unexpected result, given that the structure and morphology of MOF crystals are reported to be dependent on the solvent used in synthesis.[90−92] DMF is also a common solvent for MOF synthesis,[92,93] and octahedral CuBTC crystals as large as 70 μm have been grown in DMF.[94] It is believed that the decomposition of DMF to dimethylamine[95] allows this solvent to act as a structure directing agent in the MOF crystal

https://dx.doi.org/10.1021/acs.langmuir.0c01535
Langmuir 2020, 36, 9900−9908

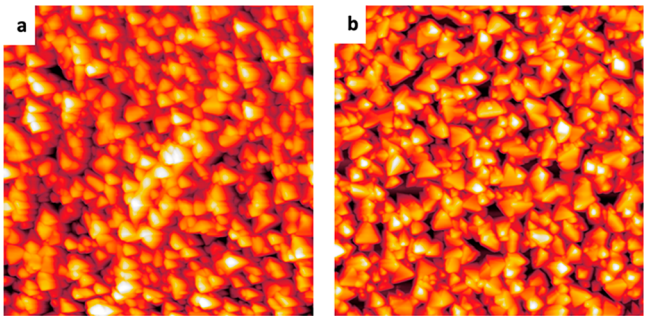

Figure 6. AFM images of the (a) CuBTC film stored at room temperature for 40 days in DMF and (b) CuCoBTC film (10% Co, exchanged at 25 °C for 60 min) stored at room temperature for 22 days in DMF. The CuBTC and CuCoBTC films were grown using 40 dip-coating cycles for the CuBTC. Both images are 5 μm × 5 μm.

growth process by controlling the basicity and extent of deprotonation of the organic carboxylate ligands.[91]

SUMMARY AND CONCLUSIONS

A novel synthesis method for producing uniform, bimetallic MOF films has been presented. CuBTC films are initially grown directly on an Al_2O_3/Si(100) substrate by a dip-coating procedure using alternating metal and ligand precursor solutions. By subsequently exposing the film to a solution of $CoCl_2$, Co^{2+} is transmetalated into the MOF structure, and the concentration of Co^{2+} can be controlled by the exchange temperature and time. The resulting CuCoBTC films retain their crystallinity, and the morphology of the crystallites covering the surface is also unchanged after Co^{2+} incorporation. To our knowledge, there have been no other reports of crystalline, bimetallic films prepared by transmetalation. This method has the advantage of allowing a wide range of metal compositions to be achieved and does not require SAM linkers to tether the MOF films to the surface, which allows for greater versatility in applications requiring higher temperatures or more reactive chemical environments. Given that the bimetallic CuMBTC MOFs are known to exhibit desirable electronic and catalytic properties as a function of metal composition, well-characterized CuMBTC films will enable detailed, fundamental studies of these properties.

ASSOCIATED CONTENT

Supporting Information

The Supporting Information is available free of charge at https://pubs.acs.org/doi/10.1021/acs.langmuir.0c0135.

Conditions for transmetalation of the CuBTC films by exposure to $CoCl_2$, XPS data for the O(1s), C(1s), and Cu(LMM) regions for the films, a cross-sectional SEM image for the CuBTC film, and AFM images from Figure 4 with vertical scale bars (PDF)

AUTHOR INFORMATION

Corresponding Authors

Donna A. Chen − *Department of Chemistry and Biochemistry, University of South Carolina, Columbia, South Carolina 29208, United States;* orcid.org/0000-0003-4962-5530; Phone: 803-777-1050; Email: dachen@sc.edu; Fax: 803-777-9521

Natalia B. Shustova − *Department of Chemistry and Biochemistry, University of South Carolina, Columbia, South Carolina 29208, United States;* orcid.org/0000-0003-3952-1949; Phone: 803-777-1903; Email: shustova@mailbox.sc.edu; Fax: 803-777-9521

Authors

Amy J. Brandt − *Department of Chemistry and Biochemistry, University of South Carolina, Columbia, South Carolina 29208, United States*

Deependra M. Shakya − *Department of Chemistry and Biochemistry, University of South Carolina, Columbia, South Carolina 29208, United States*

Kamolrat Metavarayuth − *Department of Chemistry and Biochemistry, University of South Carolina, Columbia, South Carolina 29208, United States*

Ekaterina Dolgopolova − *Department of Chemistry and Biochemistry, University of South Carolina, Columbia, South Carolina 29208, United States*

Lauren Hensley − *Department of Chemistry and Biochemistry, University of South Carolina, Columbia, South Carolina 29208, United States*

Audrey S. Duke − *Department of Chemistry and Biochemistry, University of South Carolina, Columbia, South Carolina 29208, United States*

Sharfa Farzandh − *Department of Chemistry and Biochemistry, University of South Carolina, Columbia, South Carolina 29208, United States*

Morgan Stefik − *Department of Chemistry and Biochemistry, University of South Carolina, Columbia, South Carolina 29208, United States*

Complete contact information is available at: https://pubs.acs.org/10.1021/acs.langmuir.0c01535

Notes

The authors declare no competing financial interest.

ACKNOWLEDGMENTS

This research was supported by the U.S. Department of Energy, Office of Science, Office of Basic Energy Sciences, under award DE-SC0019360. In addition, we thank the University of South Carolina's Advanced Support for Innovative Research Excellence program for funding preliminary studies. We also acknowledge USC's XPS user facility, as well as Dr. Stavros Karakalos for his help at the facility. This work made use of the South Carolina SAXS Collaborative (SCSC).

REFERENCES

(1) Lee, J.; Farha, O. K.; Roberts, J.; Scheidt, K. A.; Nguyen, S. T.; Hupp, J. T. Metal-Organic Framework Materials as Catalysts. *Chem. Soc. Rev.* **2009**, *38*, 1450−9.

(2) Chughtai, A. H.; Ahmad, N.; Younus, H. A.; Laypkov, A.; Verpoort, F. Metal-Organic Frameworks: Versatile Heterogeneous Catalysts for Efficient Catalytic Organic Transformations. *Chem. Soc. Rev.* **2015**, *44*, 6804−49.

(3) Liu, J. W.; Chen, L. F.; Cui, H.; Zhang, J. Y.; Zhang, L.; Su, C. Y. Applications of Metal-Organic Frameworks in Heterogeneous Supramolecular Catalysis. *Chem. Soc. Rev.* **2014**, *43*, 6011−61.

(4) Gascon, J.; Corma, A.; Kapteijn, F.; Llabrés i Xamena, F. X. Metal Organic Framework Catalysis: Quo Vadis? *ACS Catal.* **2014**, *4*, 361−378.

(5) Drake, T.; Ji, P. F.; Lin, W. B. Site Isolation in Metal-Organic Frameworks Enables Novel Transition Metal Catalysis. *Acc. Chem. Res.* **2018**, *51*, 2129−38.

(6) Jiao, L.; Wang, Y.; Jiang, H. L.; Xu, Q. Metal-Organic Frameworks as Platforms for Catalytic Applications. *Adv. Mater.* **2018**, *30*, 1703663.
(7) He, Y. B.; Zhou, W.; Qian, G. D.; Chen, B. L. Methane Storage in Metal-Organic Frameworks. *Chem. Soc. Rev.* **2014**, *43*, 5657−78.
(8) Herm, Z. R.; Bloch, E. D.; Long, J. R. Hydrocarbon Separations in Metal-Organic Frameworks. *Chem. Mater.* **2014**, *26*, 323−38.
(9) Furukawa, H.; Cordova, K. E.; O'Keeffe, M.; Yaghi, O. M. The Chemistry and Applications of Metal-Organic Frameworks. *Science* **2013**, *341*, 1230444.
(10) Li, J. R.; Sculley, J.; Zhou, H. C. Metal-Organic Frameworks for Separations. *Chem. Rev.* **2012**, *112*, 869−932.
(11) Phan, A.; Doonan, C. J.; Uribe-Romo, F. J.; Knobler, C. B.; O'Keeffe, M.; Yaghi, O. M. Synthesis, Structure, and Carbon Dioxide Capture Properties of Zeolitic Imidazolate Frameworks. *Acc. Chem. Res.* **2010**, *43*, 58−67.
(12) Lee, C. Y.; Farha, O. K.; Hong, B. J.; Sarjeant, A. A.; Nguyen, S. T.; Hupp, J. T. Light-Harvesting Metal-Organic Frameworks (MOFs): Efficient Strut-to-Strut Energy Transfer in Bodipy and Porphyrin-Based MOFs. *J. Am. Chem. Soc.* **2011**, *133*, 15858−61.
(13) Kent, C. A.; Mehl, B. P.; Ma, L. Q.; Papanikolas, J. M.; Meyer, T. J.; Lin, W. B. Energy Transfer Dynamics in Metal-Organic Frameworks. *J. Am. Chem. Soc.* **2010**, *132*, 12767−9.
(14) Kreno, L. E.; Leong, K.; Farha, O. K.; Allendorf, M.; Van Duyne, R. P.; Hupp, J. T. Metal-Organic Framework Materials as Chemical Sensors. *Chem. Rev.* **2012**, *112*, 1105−25.
(15) Stavila, V.; Talin, A. A.; Allendorf, M. D. MOF-Based Electronic and Optoelectronic Devices. *Chem. Soc. Rev.* **2014**, *43*, 5994−6010.
(16) Stassen, I.; Burtch, N.; Talin, A.; Falcaro, P.; Allendorf, M.; Ameloot, R. An Updated Roadmap for the Integration of Metal-Organic Frameworks with Electronic Devices and Chemical Sensors. *Chem. Soc. Rev.* **2017**, *46*, 3185−241.
(17) Dolgopolova, E. A.; Brandt, A. J.; Ejegbavwo, O. A.; Duke, A. S.; Maddumapatabandi, T. D.; Galhenage, R. P.; Larson, B. W.; Reid, O. G.; Ammal, S. C.; Heyden, A.; Chandrashekhar, M.; Stavila, V.; Chen, D. A.; Shustova, N. B. Electronic Properties of Bimetallic Metal-Organic Frameworks (MOFs): Tailoring the Density of Electronic States through MOF Modularity. *J. Am. Chem. Soc.* **2017**, *139*, 5201−9.
(18) Kobayashi, Y.; Jacobs, B.; Allendorf, M. D.; Long, J. R. Conductivity, Doping, and Redox Chemistry of a Microporous Dithiolene-Based Metal-Organic Framework. *Chem. Mater.* **2010**, *22*, 4120−2.
(19) Yang, X. C.; Xu, Q. Bimetallic Metal-Organic Frameworks for Gas Storage and Separation. *Cryst. Growth Des.* **2017**, *17*, 1450−5.
(20) Huang, Y. B.; Liang, J.; Wang, X. S.; Cao, R. Multifunctional Metal-Organic Framework Catalysts: Synergistic Catalysis and Tandem Reactions. *Chem. Soc. Rev.* **2017**, *46*, 126−57.
(21) Yuan, S.; Qin, J. S.; Li, J. L.; Huang, L.; Feng, L.; Fang, Y.; Lollar, C.; Pang, J. D.; Zhang, L. L.; Sun, D.; Alsalme, A.; Cagin, T.; Zhou, H. C. Retrosynthesis of Multi-Component Metal-Organic Frameworks. *Nat. Commun.* **2018**, *9*, 1−11.
(22) Shakya, D. M.; Ejegbavwo, O. A.; Rajeshkumar, T.; Senanayake, S. D.; Brandt, A. J.; Farzandh, S.; Acharya, N.; Ebrahim, A. M.; Frenkel, A. I.; Rui, N.; Tate, G. L.; Monnier, J. R.; Vogiatzis, K. D.; Shustova, N. B.; Chen, D. A. Selective Catalytic Chemistry at Rhodium(II) Nodes in Bimetallic Metal-Organic Frameworks. *Angew. Chem., Int. Ed.* **2019**, *58*, 16533−7.
(23) Kozachuk, O.; Luz, I.; Llabrés i Xamena, F. X.; Noei, H.; Kauer, M.; Albada, H. B.; Bloch, E. D.; Marler, B.; Wang, Y. M.; Muhler, M.; Fischer, R. A. Multifunctional, Defect-Engineered Metal-Organic Frameworks with Ruthenium Centers: Sorption and Catalytic Properties. *Angew. Chem., Int. Ed.* **2014**, *53*, 7058−7062.
(24) Beier, M. J.; Kleist, W.; Wharmby, M. T.; Kissner, R.; Kimmerle, B.; Wright, P. A.; Grunwaldt, J. D.; Baiker, A. Aerobic Epoxidation of Olefins Catalyzed by the Cobalt-Based Metal-Organic Framework STA-12(Co). *Chem. - Eur. J.* **2012**, *18*, 887−98.
(25) Ji, P. F.; Manna, K.; Lin, Z.; Feng, X. Y.; Urban, A.; Song, Y.; Lin, W. B. Single-Site Cobalt Catalysts at New $Zr_{12}(\mu_3\text{-}O)_8(\mu_3\text{-}OH)_8(\mu_2\text{-}OH)_6$ Metal-Organic Framework Nodes for Highly Active Hydrogenation of Nitroarenes, Nitriles, and Isocyanides. *J. Am. Chem. Soc.* **2017**, *139*, 7004−11.
(26) Rubio-Gimenez, V.; Galbiati, M.; Castells-Gil, J.; Almora-Barrios, N.; Navarro-Sanchez, J.; Escorcia-Ariza, G.; Mattera, M.; Arnold, T.; Rawle, J.; Tatay, S.; Coronado, E.; Marti-Gastaldo, C. Bottom-up Fabrication of Semiconductive Metal-Organic Framework Ultrathin Films. *Adv. Mater.* **2018**, *30*, 1704291.
(27) Kaur, R.; Kim, K. H.; Paul, A. K.; Deep, A. Recent Advances in the Photovoltaic Applications of Coordination Polymers and Metal Organic Frameworks. *J. Mater. Chem. A* **2016**, *4*, 3991−4002.
(28) Campbell, M. G.; Sheberla, D.; Liu, S. F.; Swager, T. M.; Dinca, M. Cu_3(Hexaiminotriphenylene)$_2$: An Electrically Conductive 2D Metal-Organic Framework for Chemiresistive Sensing. *Angew. Chem., Int. Ed.* **2015**, *54*, 4349−52.
(29) Huang, B. L.; Ni, Z.; Millward, A.; McGaughey, A. J. H.; Uher, C.; Kaviany, M.; Yaghi, O. Thermal Conductivity of a Metal-Organic Framework (MOF-5): Part II. Measurement. *Int. J. Heat Mass Transfer* **2007**, *50*, 405−11.
(30) Liu, J. X.; Woll, C. Surface-Supported Metal-Organic Framework Thin Films: Fabrication Methods, Applications, and Challenges. *Chem. Soc. Rev.* **2017**, *46*, 5730−70.
(31) Lin, S. Y.; Pineda-Galvan, Y.; Maza, W. A.; Epley, C. C.; Zhu, J.; Kessinger, M. C.; Pushkar, Y.; Morris, A. J. Electrochemical Water Oxidation by a Catalyst-Modified Metal-Organic Framework Thin Film. *ChemSusChem* **2017**, *10*, 514−22.
(32) Ye, L.; Liu, J. X.; Gao, Y.; Gong, C. H.; Addicoat, M.; Heine, T.; Woll, C.; Sun, L. C. Highly Oriented MOF Thin Film-Based Electrocatalytic Device for the Reduction of CO_2 to CO Exhibiting High Faradaic Efficiency. *J. Mater. Chem. A* **2016**, *4*, 15320−6.
(33) Wang, Y. X.; Zhao, M. T.; Ping, J. F.; Chen, B.; Cao, X. H.; Huang, Y.; Tan, C. L.; Ma, Q. L.; Wu, S. X.; Yu, Y. F.; Lu, Q. P.; Chen, J. Z.; Zhao, W.; Ying, Y. B.; Zhang, H. Bioinspired Design of Ultrathin 2D Bimetallic Metal-Organic-Framework Nanosheets Used as Biomimetic Enzymes. *Adv. Mater.* **2016**, *28*, 4149−55.
(34) Usov, P. M.; Ahrenholtz, S. R.; Maza, W. A.; Stratakes, B.; Epley, C. C.; Kessinger, M. C.; Zhu, J.; Morris, A. J. Cooperative Electrochemical Water Oxidation by Zr Nodes and Ni-Porphyrin Linkers of a PCN-224 MOF Thin Film. *J. Mater. Chem. A* **2016**, *4*, 16818−23.
(35) Shen, J. Q.; Liao, P. Q.; Zhou, D. D.; He, C. T.; Wu, J. X.; Zhang, W. X.; Zhang, J. P.; Chen, X. M. Modular and Stepwise Synthesis of a Hybrid Metal-Organic Framework for Efficient Electrocatalytic Oxygen Evolution. *J. Am. Chem. Soc.* **2017**, *139*, 1778−81.
(36) Usov, P. M.; Huffman, B.; Epley, C. C.; Kessinger, M. C.; Zhu, J.; Maza, W. A.; Morris, A. J. Study of Electrocatalytic Properties of Metal-Organic Framework PCN-223 for the Oxygen Reduction Reaction. *ACS Appl. Mater. Interfaces* **2017**, *9*, 33539−43.
(37) Wang, L.; Wu, Y. Z.; Cao, R.; Ren, L. T.; Chen, M. X.; Feng, X.; Zhou, J. W.; Wang, B. Fe/Ni Metal-Organic Frameworks and Their Binder-Free Thin Films for Efficient Oxygen Evolution with Low Overpotential. *ACS Appl. Mater. Interfaces* **2016**, *8*, 16736−43.
(38) Hod, I.; Sampson, M. D.; Deria, P.; Kubiak, C. P.; Farha, O. K.; Hupp, J. T. Fe-Porphyrin-Based Metal-Organic Framework Films as High-Surface Concentration, Heterogeneous Catalysts for Electrochemical Reduction of CO_2. *ACS Catal.* **2015**, *5*, 6302−9.
(39) Shimoni, R.; He, W. H.; Liberman, I.; Hod, I. Tuning of Redox Conductivity and Electrocatalytic Activity in Metal-Organic Framework Films Via Control of Defect Site Density. *J. Phys. Chem. C* **2019**, *123*, 5531−9.
(40) Zacher, D.; Schmid, R.; Wöll, C.; Fischer, R. A. Surface Chemistry of Metal-Organic Frameworks at the Liquid-Solid Interface. *Angew. Chem., Int. Ed.* **2011**, *50*, 176−99.
(41) Betard, A.; Fischer, R. A. Metal-Organic Framework Thin Films: From Fundamentals to Applications. *Chem. Rev.* **2012**, *112*, 1055−83.

https://dx.doi.org/10.1021/acs.langmuir.0c01535
Langmuir 2020, 36, 9900−9908

(42) Shekhah, O.; Liu, J.; Fischer, R. A.; Wöll, C. MOF Thin Films: Existing and Future Applications. *Chem. Soc. Rev.* **2011**, *40*, 1081−106.
(43) Ahrenholtz, S. R.; Epley, C. C.; Morris, A. J. Solvothermal Preparation of an Electrocatalytic Metalloporphyrin MOF Thin Film and Its Redox Hopping Charge-Transfer Mechanism. *J. Am. Chem. Soc.* **2014**, *136*, 2464−72.
(44) Kung, C. W.; Chang, T. H.; Chou, L. Y.; Hupp, J. T.; Farha, O. K.; Ho, K. C. Post Metalation of Solvothermally Grown Electroactive Porphyrin Metal-Organic Framework Thin Films. *Chem. Commun.* **2015**, *51*, 2414−7.
(45) Zhao, S. L.; Wang, Y.; Dong, J. C.; He, C. T.; Yin, H. J.; An, P. F.; Zhao, K.; Zhang, X. F.; Gao, C.; Zhang, L. J.; Lv, J. W.; Wang, J. X.; Zhang, J. Q.; Khattak, A. M.; Khan, N. A.; Wei, Z. X.; Zhang, J.; Liu, S. Q.; Zhao, H. J.; Tang, Z. Y. Ultrathin Metal-Organic Framework Nanosheets for Electrocatalytic Oxygen Evolution. *Nat. Energy* **2016**, *1*, 1−10.
(46) Summerfield, A.; Cebula, I.; Schroder, M.; Beton, P. H. Nucleation and Early Stages of Layer-by-Layer Growth of Metal Organic Frameworks on Surfaces. *J. Phys. Chem. C* **2015**, *119*, 23544−51.
(47) Shekhah, O.; Wang, H.; Kowarik, S.; Schreiber, F.; Paulus, M.; Tolan, M.; Sternemann, C.; Evers, F.; Zacher, D.; Fischer, R. A.; Wöll, C. Step-by-Step Route for the Synthesis of Metal-Organic Frameworks. *J. Am. Chem. Soc.* **2007**, *129*, 15118−9.
(48) Kind, M.; Wöll, C. Organic Surfaces Exposed by Self-Assembled Organothiol Monolayers: Preparation, Characterization, and Application. *Prog. Surf. Sci.* **2009**, *84*, 230−78.
(49) Shekhah, O.; Wang, H.; Strunskus, T.; Cyganik, P.; Zacher, D.; Fischer, R.; Wöll, C. Layer-by-Layer Growth of Oriented Metal Organic Polymers on a Functionalized Organic Surface. *Langmuir* **2007**, *23*, 7440−2.
(50) Shekhah, O.; Wang, H.; Zacher, D.; Fischer, R. A.; Wöll, C. Growth Mechanism of Metal-Organic Frameworks: Insights into the Nucleation by Employing a Step-by-Step Route. *Angew. Chem., Int. Ed.* **2009**, *48*, 5038−41.
(51) Gliemann, H.; Woll, C. Epitaxially Grown Metal-Organic Frameworks. *Mater. Today* **2012**, *15*, 110−6.
(52) Heinke, L.; Woll, C. Surface-Mounted Metal-Organic Frameworks: Crystalline and Porous Molecular Assemblies for Fundamental Insights and Advanced Applications. *Adv. Mater.* **2019**, *31*, 1806324.
(53) Haldar, R.; Heinke, L.; Woll, C. Advanced Photoresponsive Materials Using the Metal-Organic Framework Approach. *Adv. Mater.* **2020**, *32*, 1905227.
(54) Wang, Y. M.; Woll, C. Chemical Reactions at Isolated Single-Sites inside Metal-Organic Frameworks. *Catal. Lett.* **2018**, *148*, 2201−22.
(55) Falcaro, P.; Ricco, R.; Doherty, C. M.; Liang, K.; Hill, A. J.; Styles, M. J. MOF Positioning Technology and Device Fabrication. *Chem. Soc. Rev.* **2014**, *43*, 5513−60.
(56) Zheng, F. Q.; Xiang, D.; Li, P.; Zhang, Z. W.; Du, C.; Zhuang, Z. H.; Li, X. K.; Chen, W. Highly Conductive Bimetallic Ni-Fe Metal Organic Framework as a Novel Electrocatalyst for Water Oxidation. *ACS Sustainable Chem. Eng.* **2019**, *7*, 9743−9.
(57) Simons, M. C.; Ortuno, M. A.; Bernales, V.; Gaggioli, C. A.; Cramer, C. J.; Bhan, A.; Gagliardi, L. C-H Bond Activation on Bimetallic Two-Atom Co-M Oxide Clusters Deposited on Zr-Based MOF Nodes: Effects of Doping at the Molecular Level. *ACS Catal.* **2018**, *8*, 2864−9.
(58) Kim, D.; Song, K. S.; Buyukcakir, O.; Yildirim, T.; Coskun, A. Bimetallic Metal Organic Frameworks with Precisely Positioned Metal Centers for Efficient H_2 Storage. *Chem. Commun.* **2018**, *54*, 12218−21.
(59) Islamoglu, T.; Goswami, S.; Li, Z. Y.; Howarth, A. J.; Farha, O. K.; Hupp, J. T. Postsynthetic Tuning of Metal-Organic Frameworks for Targeted Applications. *Acc. Chem. Res.* **2017**, *50*, 805−13.
(60) Kung, C. W.; Mondloch, J. E.; Wang, T. C.; Bury, W.; Hoffeditz, W.; Klahr, B. M.; Klet, R. C.; Pellin, M. J.; Farha, O. K.; Hupp, J. T. Metal-Organic Framework Thin Films as Platforms for Atomic Layer Deposition of Cobalt Ions to Enable Electrocatalytic Water Oxidation. *ACS Appl. Mater. Interfaces* **2015**, *7*, 28223−30.
(61) Otake, K. I.; Cui, Y. X.; Buru, C. T.; Li, Z. Y.; Hupp, J. T.; Farha, O. K. Single-Atom-Based Vanadium Oxide Catalysts Supported on Metal Organic Frameworks: Selective Alcohol Oxidation and Structure Activity Relationship. *J. Am. Chem. Soc.* **2018**, *140*, 8652−6.
(62) Platero-Prats, A. E.; League, A. B.; Bernales, V.; Ye, J. Y.; Gallington, L. C.; Vjunov, A.; Schweitzer, N. M.; Li, Z. Y.; Zheng, J.; Mehdi, B. L.; Stevens, A. J.; Dohnalkova, A.; Balasubramanian, M.; Farha, O. K.; Hupp, J. T.; Browning, N. D.; Fulton, J. L.; Camaioni, D. M.; Lercher, J. A.; Truhlar, D. G.; Gagliardi, L.; Cramer, C. J.; Chapman, K. W. Bridging Zirconia Nodes within a Metal-Organic Framework Via Catalytic Ni-Hydroxo Clusters to Form Heterobimetallic Nanowires. *J. Am. Chem. Soc.* **2017**, *139*, 10410−8.
(63) Liu, J.; Ye, J. Y.; Li, Z. Y.; Otake, K.; Liao, Y. J.; Peters, A. W.; Noh, H.; Truhlar, D. G.; Gagliardi, L.; Cramer, C. J.; Farha, O. K.; Hupp, J. T. Beyond the Active Site: Tuning the Activity and Selectivity of a Metal-Organic Framework-Supported Ni Catalyst for Ethylene Dimerization. *J. Am. Chem. Soc.* **2018**, *140*, 11174−8.
(64) Duan, J. J.; Chen, S.; Zhao, C. Ultrathin Metal-Organic Framework Array for Efficient Electrocatalytic Water Splitting. *Nat. Commun.* **2017**, *8*, 15341.
(65) Sakaida, S.; Haraguchi, T.; Otsubo, K.; Sakata, O.; Fujiwara, A.; Kitagawa, H. Fabrication and Structural Characterization of an Ultrathin. Film of a Two-Dimensional-Layered Metal-Organic Framework, $\{Fe(Py)_2\ Ni(CN)_4\}$ (Py = Pyridine). *Inorg. Chem.* **2017**, *56*, 7606−9.
(66) Haraguchi, T.; Otsubo, K.; Sakata, O.; Fujiwara, A.; Kitagawa, H. Remarkable Lattice Shrinkage in Highly Oriented Crystalline Three-Dimensional Metal-Organic Framework Thin Films. *Inorg. Chem.* **2015**, *54*, 11593−5.
(67) Otsubo, K.; Haraguchi, T.; Sakata, O.; Fujiwara, A.; Kitagawa, H. Step-by-Step Fabrication of a Highly Oriented Crystalline Three-Dimensional Pillared-Layer-Type Metal-Organic Framework Thin Film Confirmed by Synchrotron X-ray Diffraction. *J. Am. Chem. Soc.* **2012**, *134*, 9605−8.
(68) Haraguchi, T.; Otsubo, K.; Sakata, O.; Kawaguchi, S.; Fujiwara, A.; Kitagawa, H. A Three-Dimensional Accordion-Like Metal Organic Framework: Synthesis and Unconventional Oriented Growth on a Surface. *Chem. Commun.* **2016**, *52*, 6017−20.
(69) Sakaida, S.; Otsubo, K.; Sakata, O.; Song, C.; Fujiwara, A.; Takata, M.; Kitagawa, H. Crystalline Coordination Framework Endowed with Dynamic Gate-Opening Behaviour by Being Downsized to a Thin Film. *Nat. Chem.* **2016**, *8*, 377−83.
(70) Gotthardt, M. A.; Schoch, R.; Wolf, S.; Bauer, M.; Kleist, W. Synthesis and Characterization of Bimetallic Metal-Organic Framework Cu-Ru-BTC with HKUST-1 Structure. *Dalton Trans.* **2015**, *44*, 2052−6.
(71) Chui, S. S. Y.; Lo, S. M. F.; Charmant, J. P. H.; Orpen, A. G.; Williams, I. D. A Chemically Functionalizable Nanoporous Material $[Cu_3(TMa)_2(H_2O)_3]_N$. *Science* **1999**, *283*, 1148−50.
(72) Stavila, V.; Volponi, J.; Katzenmeyer, A. M.; Dixon, M. C.; Allendorf, M. D. Kinetics and Mechanism of Metal-Organic Framework Thin Film Growth: Systematic Investigation of HKUST-1 Deposition on QCM Electrodes. *Chem. Sci.* **2012**, *3*, 1531−40.
(73) Bradshaw, D.; Garai, A.; Huo, J. Metal-Organic Framework Growth at Functional Interfaces: Thin Films and Composites for Diverse Applications. *Chem. Soc. Rev.* **2012**, *41*, 2344−81.
(74) Biemmi, E.; Scherb, C.; Bein, T. Oriented Growth of the Metal Organic Framework $Cu_3(BTC)_2(H_2O)_3{\cdot}xH_2O$ Tunable with Functionalized Self-Assembled Monolayers. *J. Am. Chem. Soc.* **2007**, *129*, 8054−5.
(75) Xu, Q.; Li, H.; Yue, F.; Chi, L.; Wang, J. D. Nanoscale Cobalt Metal-Organic Framework as a Catalyst for Visible Light-Driven and Electrocatalytic Water Oxidation. *New J. Chem.* **2016**, *40*, 3032−5.
(76) Duke, A. S.; Dolgopolova, E. A.; Galhenage, R. P.; Ammal, S. C.; Heyden, A.; Smith, M. D.; Chen, D. A.; Shustova, N. B. Active

https://dx.doi.org/10.1021/acs.langmuir.0c01535
Langmuir 2020, 36, 9900−9908

Sites in Copper-Based Metal Organic Frameworks: Understanding Substrate Dynamics, Redox Processes, and Valence Band Structure. *J. Phys. Chem. C* **2015**, *119*, 27457−66.
(77) Vaz, C. A. F.; Prabhakaran, D.; Altman, E. I.; Henrich, V. E. Experimental Study of the Interfacial Cobalt Oxide in Co_3O_4/Alpha-Al_2O_3(0001) Epitaxial Films. *Phys. Rev. B: Condens. Matter Mater. Phys.* **2009**, *80*, 155457.
(78) Kochubey, D.; Kaichev, V.; Saraev, A.; Tomyn, S.; Belov, A.; Voloshin, Y. Combined X-ray Absorption Near-Edge Structure and X-ray Photoelectron Study of the Electrocatalytically Active Cobalt(I) Cage Complexes and the Clathrochelate Cobalt(II)- and Cobalt(III)-Containing Precursors and Analogs. *J. Phys. Chem. C* **2013**, *117*, 2753−9.
(79) Brown, D. G.; Weser, U. XPS Spectra of Spin-Triplet Cobalt(III) Complexes. *Z. Naturforsch., B: J. Chem. Sci.* **1979**, *34*, 1468−70.
(80) Andersson, S. L. T.; Howe, R. F. An X-Ray Photoelectron Study of Metal-Clusters in Zeolites. *J. Phys. Chem.* **1989**, *93*, 4913−20.
(81) Frost, D. C.; McDowell, C. A.; Woolsey, I. S. Evidence for Multiplet Splitting of 2p Photoelectron Lines of Transition-Metal Complexes. *Chem. Phys. Lett.* **1972**, *17*, 320−3.
(82) Haraguchi, H.; Fujiwara, K.; Fuwa, K. A Study of Cobalt Complexes by X-ray Photoelectron Spectroscopy. *Chem. Lett.* **1975**, *4*, 409−14.
(83) Nijem, N.; Bluhm, H.; Ng, M. L.; Kunz, M.; Leone, S. R.; Gilles, M. K. Cu^{1+} in HKUST-1: Selective Gas Adsorption in the Presence of Water. *Chem. Commun.* **2014**, *50*, 10144−7.
(84) Wagner, C. D.; Riggs, W. M.; Davis, L. E.; Moulder, J. F. *Handbook of X-ray Photoelectron Spectroscopy*; Perkin Elmer Corporation: Eden Prairie, MN, 1979.
(85) Ghijsen, J.; Tjeng, L. H.; Vanelp, J.; Eskes, H.; Westerink, J.; Sawatzky, G. A.; Czyzyk, M. T. Electronic-Structure of Cu_2O and CuO. *Phys. Rev. B: Condens. Matter Mater. Phys.* **1988**, *38*, 11322−30.
(86) Deroubaix, G.; Marcus, P. X-Ray Photoelectron-Spectroscopy Analysis of Copper and Zinc-Oxides and Sulfides. *Surf. Interface Anal.* **1992**, *18*, 39−46.
(87) Yao, Q. X.; Sun, J. L.; Li, K.; Su, J.; Peskov, M. V.; Zou, X. D. A Series of Isostructural Mesoporous Metal-Organic Frameworks Obtained by Ion-Exchange Induced Single-Crystal to Single-Crystal Transformation. *Dalton Trans.* **2012**, *41*, 3953−5.
(88) Tian, F. P.; Qiao, C. X.; Zheng, R. Y.; Ru, Q. F.; Sun, X.; Zhang, Y. F.; Meng, C. G. Synthesis of Bimetallic-Organic Framework Cu/Co-BTC and the Improved Performance of Thiophene Adsorption. *RSC Adv.* **2019**, *9*, 15642−7.
(89) Teo, J. M.; Coghlan, C. J.; Evans, J. D.; Tsivion, E.; Head-Gordon, M.; Sumby, C. J.; Doonan, C. J. Hetero-Bimetallic Metal-Organic Polyhedra. *Chem. Commun.* **2016**, *52*, 276−9.
(90) Kamakura, Y.; Hosono, N.; Terashima, A.; Kitagawa, S.; Yoshikawa, H.; Tanaka, D. Atomic Force Microscopy Study of the Influence of the Synthesis Conditions on the Single-Crystal Surface of Interdigitated Metal-Organic Frameworks. *ChemPhysChem* **2018**, *19*, 2134−8.
(91) Seetharaj, R.; Vandana, P. V.; Arya, P.; Mathew, S. Dependence of Solvents, pH, Molar Ratio and Temperature in Tuning Metal Organic Framework Architecture. *Arabian J. Chem.* **2019**, *12*, 295−315.
(92) Seoane, B.; Castellanos, S.; Dikhtiarenko, A.; Kapteijn, F.; Gascon, J. Multi-Scale Crystal Engineering of Metal Organic Frameworks. *Coord. Chem. Rev.* **2016**, *307*, 147−87.
(93) Farha, O. K.; Hupp, J. T. Rational Design, Synthesis, Purification, and Activation of Metal-Organic Framework Materials. *Acc. Chem. Res.* **2010**, *43*, 1166−75.
(94) Shöâeè, M.; Agger, J. R.; Anderson, M. W.; Attfield, M. P. Crystal Form, Defects and Growth of the Metal Organic Framework HKUST-1 Revealed by Atomic Force Microscopy. *CrystEngComm* **2008**, *10*, 646−8.
(95) Muzart, J. N,N-Dimethylformamide: Much More Than a Solvent. *Tetrahedron* **2009**, *65*, 8313−23.

https://dx.doi.org/10.1021/acs.langmuir.0c01535
Langmuir 2020, 36, 9900−9908